Journal of Electrochemistry

Volume 23
Issue 2 *Special Issue in Honor of Professor Zhaowu Tian on His 90th Birthday*

2017-04-28

Comparative Studies of Fe, Ni, Co and Their Bimetallic Nanoparticles for Electrochemical Water Oxidation

Maduraiveeran Govindhan

Brennan Mao

Aicheng Chen
Department of Chemistry, Lakehead University, 955 Oliver Road, Thunder Bay, Ontario P7B 5E1, Canada;,
aicheng.chen@lakeheadu.ca

Recommended Citation

Maduraiveeran Govindhan, Brennan Mao, Aicheng Chen. Comparative Studies of Fe, Ni, Co and Their Bimetallic Nanoparticles for Electrochemical Water Oxidation[J]. *Journal of Electrochemistry*, 2017 , 23(2): 159-169.
DOI: 10.13208/j.electrochem.161247
Available at: https://jelectrochem.xmu.edu.cn/journal/vol23/iss2/6

DOI: 10.13208/j.electrochem.161247 **Artical ID**:1006-3471(2017)02-0159-11
Cite this: *J. Electrochem.* **2017**, *23*(2): 159-169 **Http**://electrochem.xmu.edu.cn

Comparative Studies of Fe, Ni, Co and Their Bimetallic Nanoparticles for Electrochemical Water Oxidation

Maduraiveeran Govindhan, Brennan Mao, Aicheng Chen*
(*Department of Chemistry, Lakehead University*, 955 *Oliver Road, Thunder Bay, Ontario* P7B 5E1, *Canada*)

Abstract: The design of efficient, durable, and earth-abundant electrocatalysts via environmentally compatible strategies for the oxygen evolution reaction (OER) is a vital for energy conversion processes. Herein we report a facile approach for the fabrication of low-cost and earth abundant metal catalysts, including iron (Fe), nickel (Ni), cobalt (Co), CoNi, and CoFe nanoparticles (NPs) on titanium (Ti) substrates through a one-step electrochemical deposition. Field-emission scanning electron microscopy(FE-SEM), energy dispersive X-ray spectroscopy (EDX), X-ray diffraction (XRD) spectrocopy, X-ray photoelectron spectroscopy (XPS), and electrochemical techniques were employed to characterize these nanoparticles. Our electrochemical results revealed that among the five synthesized nanomaterials, the Ti/Co electrode exhibited the highest electrocatalytic activity toward OER in 0.l mol·L^{-1} KOH with a current density of 10.0 mA·cm^{-2} at 0.70 V vs. Ag/AgCl. The optimized Ti/Co electrode exhibited a small overpotential (η) of 0.43 V at 10.0 mA·cm^{-2} and a high mass activity of 105.7 A·g^{-1} with a turnover frequency (TOF) value of 1.63×10^{-3} s^{-1}, which are comparable to the values obtained with the state-of-the-art Pt/C and RuO_2 electrocatalysts. In addition, the durability of the optimized Ti/Co electrode was tested using a chronopotentiometric technique, which revealed that the developed electrocatalyst possessed good stability for OER in an alkaline solution. The high catalytic activity, high stability, earth abundance, cost-effectiveness, and easy scale-up for mass production make the Co nanoparticles, which were electrochemically deposited on a Ti substrate, promising for industrial water splitting.

Key words: cobalt nanoparticle; electrochemical deposition; electrocatalyst; oxygen evolution reaction; energy conversion
CLC Number: O646 **Document Code**: A

The development of a technology that has the capacity to efficiently generate hydrogen from water would provide a new renewable, sustainable, and clean energy system to address the critical climate change and environmental issues, which are caused by the combustion of coal, oil, and natural gas [1-3]. Electrochemical water oxidation is one of the potential approaches for the production of hydrogen on an industrial scale, although more cost-effective and efficient electrocatalysts for the oxygen evolution reaction (OER) are required to be developed[4-6]. The electrochemical water splitting process is comprised of two key reactions: OER at the anode, and hydrogen evolution reaction (HER) at the cathode. However, the OER (e.g., 4 $OH^- \rightarrow 2H_2O + 4e + O_2$, occurring in an alkaline solution) exhibits sluggish kinetics, which constrains the efficiency of water splitting devices[7-9]. Robust and highly active electrocatalysts are thus required in order to lower the overpotential (η) and improve the overall efficiency of the OER.

In a water electrolysis system, the overpotential, which is related to the electrode potential difference and is essential for driving the reaction at a given current density, is primarily from the OER rather than initiated by the HER[4,10]. Several hundred millivolts of overpotential are often required to be overcome, toward the achievement of a typical current density of 10.0 mA·cm^{-2}[11-13]. For this reason, considerable research efforts have been invested in the development of high-performance electrocatalysts with low OER overpotential and cost. Currently, precious metals (e.g., Pt, PtIr, PtRu) and metal oxides such as RuO_2 and

Received: 2016-12-17, Revised: 2017-03-21 *Corresponding author, Tel: 1 807 343 8318 , E-mail: aicheng.chen@lakeheadu.ca

IrO_2 are considered to be state-of-the-art electrocatalysts for the OER[13-14]. Unfortunately, these are among the rarest elements on earth and are costly; hence, it is not practical to employ them for large-scale commercial electrochemical water splitting[14-16]. Consequently, there are great interests in the development of earth abundant metal and metal oxide based electrocatalysts with high specific surface areas for the OER[1,17-19]. Recent studies have shown that nickel (Ni), iron (Fe), and cobalt (Co) based metal/oxides, hydro(oxy)oxides, phosphates, chalcogenides and perovskites are promising for the OER due to their high catalytic activity, earth abundance, and low cost[20-25]. There are several methods available for the preparation of stable electrocatalysts, including electrodeposition, hydrothermal, and chemical reduction methods. Hydrothermal and chemical reduction methods may potentially exhibit high-performance for OER, but they possess a number of disadvantages, including high temperature, lengthy operation time, and the use of toxic reducing chemicals in the formation of non-noble metal nanostructures.

Electrochemical deposition comprises a green approach that may produce mono-dispersed nanomaterials with high active surface areas onto substrate surfaces. The morphology and thickness of active electrocatalysts can be simply controlled by manipulating the current or charge applied to the electrodes[26-29]. Many researchers have been intensively investigating the enhanced performance of electrocatalysts by altering preparation methods, annealing conditions, dispersion techniques, precursors and solvents, and current or charge to achieve highly active surface areas and stable catalytic responses. In the present study, we directly grew a series of non-noble metal electrocatalysts, including Fe, Ni, Co, CoNi, and CoFe NPs on a Ti substrate, via a one-step facile electrochemical deposition method. A Ti plate was selected as the electrode substrate due to its low cost, high mechanical and thermal stability, and high corrosion resistivity, which are very important for practical applications. Our experimental results revealed that a Ti/Co electrode possessed high OER electrocatalytic performance over the other electrodes fabricated in the present study. The optimized Ti/Co electrode exhibited a lower η and smaller Tafel slope in contrast to a benchmark Pt electrocatalyst in alkaline media. To the best of our knowledge, this is the first report on the deposition of Co NPs on a Ti substrate as an efficient electrocatalyst for water oxidation. The cost-effectiveness, high catalytic activity and easy scale-up for manufacturability make the nanostructured Ti/Co electrode developed in the present study promising for practical energy applications.

1 Experimental

1.1 Materials

Analytical grade cobalt(II) sulfate heptahydrate, nickel(II) nitrate hexahydrate, iron(III) nitrate hexahydrate, and potassium hydroxide (KOH) were purchased from Sigma-Aldrich. Ti plates (99.2%, 1.25 cm × 0.80 cm × 0.5 mm) were cleaned by sonication in acetone, followed by pure water (18.2 MΩ·cm), then etched in an 18% HCl solution at 85 ℃ for 10 min, and finally copiously rinsed with pure water. All other analytical grade reagents were used as received. Double distilled water, purified with a NANOpure® water system was used in the preparation of all solutions. All electrochemical experiments were carried out in a 0.1 mol·L^{-1} KOH electrolyte solution.

1.2 Fabrication and Characterization

The Fe, Ni, Co, CoNi, and CoFe NPs were grown directly onto the Ti substrate using a single-step electrochemical deposition method. The electrochemical deposition of the non-noble metal nanoparticles was carried out by applying the electrode potential of -1.0 V (vs. Ag/AgCl) for 10 min in an Ar-saturated 5 mmol·L^{-1} metal salt + 0.1 mol·L^{-1} Na_2SO_4 solution. The resulting electrode was rinsed with a copious amount of water and dried at 40 ℃ in an oven. To optimize the quantity of Co NPs formed on the Ti substrate, the electrodeposition time was varied from 2 to 15 min. Morphological and energy dispersive X-ray spectroscopic (EDX) studies were performed utilizing a field emission scanning electron microscope (FE-SEM) (Hitachi SU-70). X-ray diffraction (XRD) patterns were recorded using a Pananalyt-

ical Xpert Pro Diffractometer with a Ni filtered monochromatic Cu Kr (0.15406 nm, 2.2 kW Max.). X-ray photoelectron spectra (XPS) were recorded via a ThermoFisher XPS system, where the size of the X-ray spot was 400 μm, using an Al K_α monochromatic source.

Electrochemical experiments were performed with a CHI 660B electrochemical workstation (CH Instrument Inc. USA) utilizing a conventional one compartment three-electrode cell. The nanoparticles deposited on the Ti substrate were utilized as the working electrode, whereas silver/silver chloride (Ag/AgCl) was utilized as the reference electrode, and a platinum coil was used as the counter electrode. Argon (Ar) gas was introduced to purge the solution in achieving an O_2-free condition. All of the electrochemical experiments were performed at ambient room temperature (20 ± 2 ℃). OER was carried out in a 0.1 mol·L^{-1} KOH electrolyte, which was purged with high purity Ar for 20 min to remove all of the dissolved oxygen. Linear sweep voltammetric (LSV) experiments were performed by sweeping the potential from 0.0 to 1.0 V for several scans until a stable LSV curve was obtained.

2 Results and Discussion

The surface morphologies of the Fe, Ni, Co, CoNi, and CoFe NPs deposited on the Ti substrates were characterized by FE-SEM. As seen in the SEM images (Figs. 1A-E), nanoparticles with different morphologies and dimensions were successfully formed via a single-step electrochemical deposition approach under a constant applied electrode potential of -1.0 V (vs. Ag/AgCl) for 10 min. Fig. 1A shows the FE-SEM image of the formed Fe NPs with an average nanoparticle size of ~ 370 nm, which exhibited the largest size due to agglomeration in comparison to all of the other nanoparticles deposited on the Ti substrate. As depicted in Fig. 1B, the Ni NPs were uniformly distributed on the substrate, and their average particle size was calculated to be ~ 28 nm, which was smaller than those of the Co and Fe NPs. Fig. 1C presents the FE-SEM image of the Co NPs with an average particle size of ~ 31 nm. The formed Co NPs were covered with thin Co layers, which linked different nanoparticles together. As shown in Fig. 1D the formed bimetallic CoNi NPs exhibited a cubic shape with an average nanoparticle size of ~ 67 nm, which were different from the prepared Ni and Co NPs. In addition, heterogeneous CoFe nanostructures with various shapes such as rods, triangles, cubes, and spheres were deposited on the Ti substrates as displayed in Fig. 1E. For instance, the nanorods had average lengths of ~ 48 nm and diameters of ~ 15 nm; and the median dimension of the spherically shaped nanoparticles was measured to be ~ 44 nm. Fig. 1F presents the EDX spectra of the Ti/Fe, Ti/Ni, Ti/Co, Ti/CoNi, and Ti/CoFe electrodes, which confirmed their compositions. The atomic ratios of Co:Ni and Co:Fe were calculated to be 40.6:59.4 (1.0:1.4) and 44.9:55.1 (1.0:1.2) for the bimetallic CoNi and CoFe nanoparticles deposited on the Ti substrates, respectively. The different ratios could be attributed to their different electrochemical reduction potentials, as well as how the nanoparticles were formed on the Ti substrates.

The fabricated Ti, Ti/Fe, Ti/Ni, Ti/Co, Ti/CoNi,

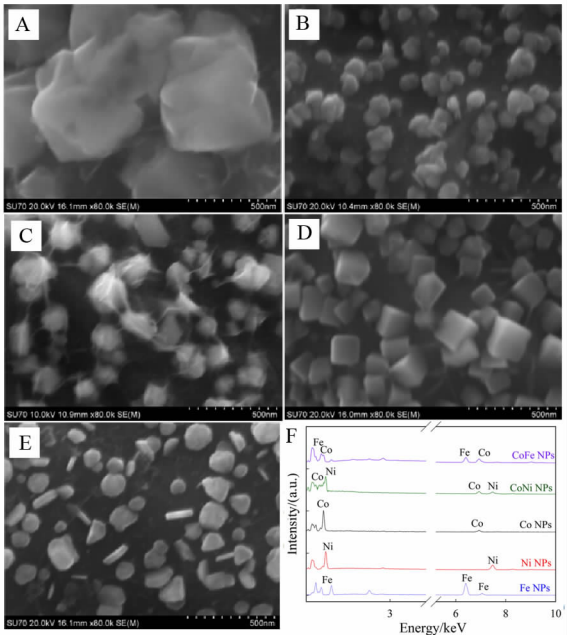

Fig. 1 FE-SEM images of the Fe NPs (A), Ni NPs (B), Co NPs (C), CoNi NPs (D) and CoFe NPs (E). EDX spectra of the Fe NPs, Ni NPs, Co NPs, CoNi NPs and CoFe NPs (F).

and Ti/CoFe electrodes were tested toward the electrocatalytic oxidation of water in 0.1 mol·L^{-1} KOH. Fig. 2A displays the LSV curves of these six electrodes, whereas their corresponding current densities measured at 1.0 V. As anticipated, the unmodified Ti electrode had minimal catalytic activity; almost no OER response was observed in the investigated electrode potential range. As seen in Fig. 2A, the onset potential for the OER was decreased in the following order: Ti > Ti/Ni > Ti/CoNi ≈ Ti/Fe > Ti/CoFe ≈ Ti/Co electrodes. The current density was increased in the following order: Ti < Ti/Ni < Ti/CoNi < Ti/Fe < Ti/CoFe < Ti/Co electrodes, revealing that the formed Co NPs possessed the highest catalytic activity for the OER. At 1.0 V, the current density of the Ti/Co electrode was 62.6 mA·cm^{-2}, which was ~ 52.2 and ~ 7.6 times higher than those of the Ti/Ni (1.2 mA·cm^{-2}) and Ti/Fe (8.2 mA·cm^{-2}), respectively. Fig. 2B presents the Tafel plots of the Ti electrodes modified with the different nanomaterials, indicating that the Tafel slope was decreased in the following order: Ti/Ni (147 mV·dec^{-1}) > Ti/CoNi (138 mV·dec^{-1}) > Ti/Fe (131 mV·dec^{-1}) > Ti/CoFe (86 mV·dec^{-1}) > Ti/Co (81 mV·dec^{-1}) electrodes. These aforementioned results revealed that although the formations of the CoNi and CoFe NPs improved the catalytic activities of the Ni and Fe NPs, the bimetallic NPs still exhibited lower activity than the formed Co NPs. Thus, we focused primarily on the characterization, optimization and testing of the Co NPs in the subsequent study and discussion.

The crystalline nature, surface chemical composition and valence states of the Co NPs deposited on the Ti substrate were further examined using XRD and XPS. Fig. 3A shows the XRD pattern of the Ti/Co electrode surface, where the peaks marked with asterisks were derived from the Ti substrate. Two sharp diffraction peaks centered at 44.4° and 51.9° appeared, which were indexed to the (111) and

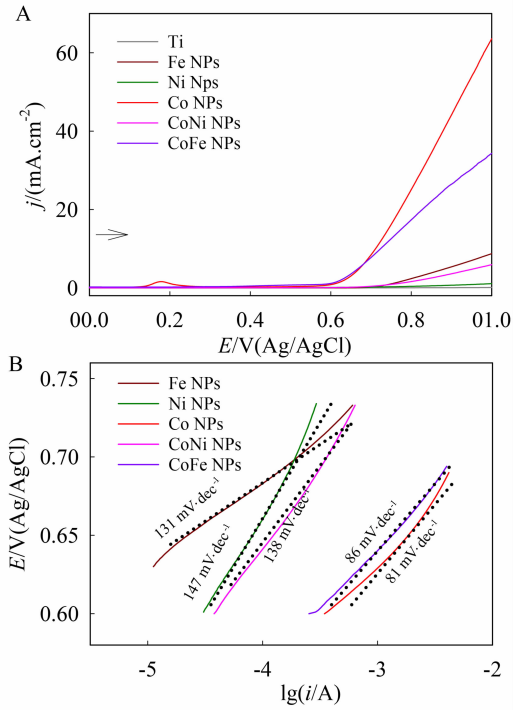

Fig. 2 A. LSV curves of the Ti, Ti/Fe, Ti/Ni, Ti/Co, Ti/CoNi and Ti/CoFe electrodes recorded in 0.1 mol·L^{-1} KOH at a scan rate of 20 mV·s^{-1}; B. Tafel plots of the Ti/Fe, Ti/Ni, Ti/Co, Ti/CoNi and Ti/CoFe electrodes recorded in 0.1 mol·L^{-1} KOH at the scan rate of 0.1 mV·s^{-1}.

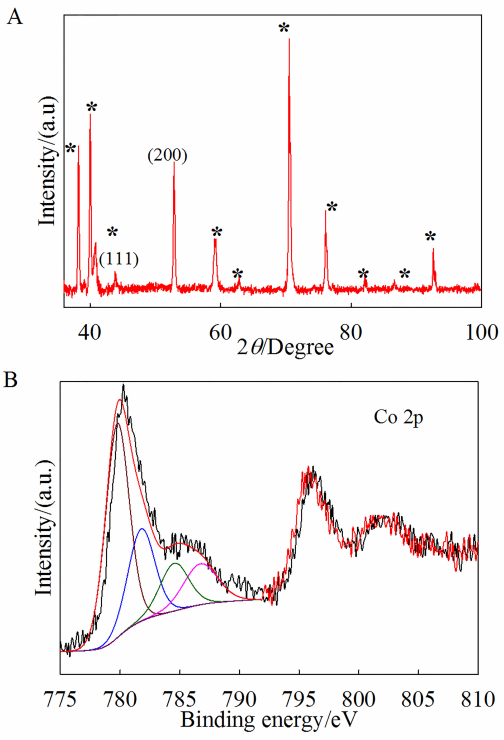

Fig. 3 A. XRD pattern of the Ti/Co-10 electrode. The peaks marked with asterisks were derived from Ti substrate; B. XPS data of Co 2p recorded for the Ti/Co-10 electrode

(200) reflections of the face-centered cubic (fcc) structure of metallic cobalt (JCPDS File No: 15-0806). This result was consistent with the previous reports on metallic Co[30]. Fig. 3B depicts the Co 2p XPS of the Ti/Co electrode; the peaks appeared at ~ 799.6 and ~ 796.9 eV, which corresponded to the Co $2p^{3/2}$ and Co $2p^{1/2}$ states. The binding energies were shifted from the metallic Co $2p^{3/2}$ (778.1 eV) and Co $2p^{1/2}$ (793.3 eV), indicating that the metallic Co NPs deposited on the Ti substrate were partially oxidized with oxygen in the surrounding[30].

The quantity of the Co NPs deposited on the Ti substrate was optimized by changing the electrochemical deposition periods to 2, 5, 10, and 15 min at an applied electrode potential of -1.0 V vs. Ag/AgCl; and the obtained Ti/Co electrodes were designated as Ti/Co-2, Ti/Co-5, Ti/Co-10, and Ti/Co-15, respectively. Fig. 4A depicts the LSV curves of the Ti/Co-2, Ti/Co-5, Ti/Co-10, and Ti/Co-15 electrodes recorded in 0.1 mol·L^{-1} KOH, while Figs. 4B and 4C present the corresponding plots of the current densities measured at 1.0 V and an electrode potential at 10.0 mA·cm^{-2} versus the as-prepared Ti/Co electrodes. With an increase of the electrodeposition time from 2 to 10 min, the current density was raised. This might have been attributed to the formation of the highly densed and interconnected Co NPs on the Ti surface, as shown in Fig. 1C, providing additional catalytic active sites for water oxidation. However, further increasing the electrodeposition time to 15 min the current density was slightly decreased. The excess Co deposition might have led to the formation of larger particles, thus decreasing the population of active sites for the OER. As compared in Figs. 4B & C and Table 1, the prepared Ti/Co-10 electrode exhibited the lowest onset potential (0.56 V), the least oxidation potential (0.70 V) to achieve a current density of 10.0 mA·cm^{-2}, and the highest current density (62.6 mA·cm^{-2}) at the applied electrode potential of 1.0 V, showing that 10 min was the optimized electrodeposition time.

Electrochemical impedance spectroscopic (EIS) measurements were made to further investigate the electrocatalytic activity of the prepared Ti/Co electrodes for OER. Fig. 5 displays the Nyquist plots of the Ti/Co-2 (a), Ti/Co-5 (b), Ti/Co-10 (c), and Ti/Co-15 (d) electrodes recorded in 0.1 mol·L^{-1} KOH at an applied potential of 0.6 V. The Nyquist plot of the complex impedance represents the imaginary versus the actual portion of the impedance, and the formed semicircles in the applied frequencies corresponded to the electron transfer-limited process. The inset in Fig. 5 displays an equivalent electric circuit to fit the obtained EIS experimental data, where R_s denotes the solution resistance, R_p the charge-transfer resistance and CPE the constant phase element which is defined by CPE-T and CPE-P. The CPE is considered to be a capacitor

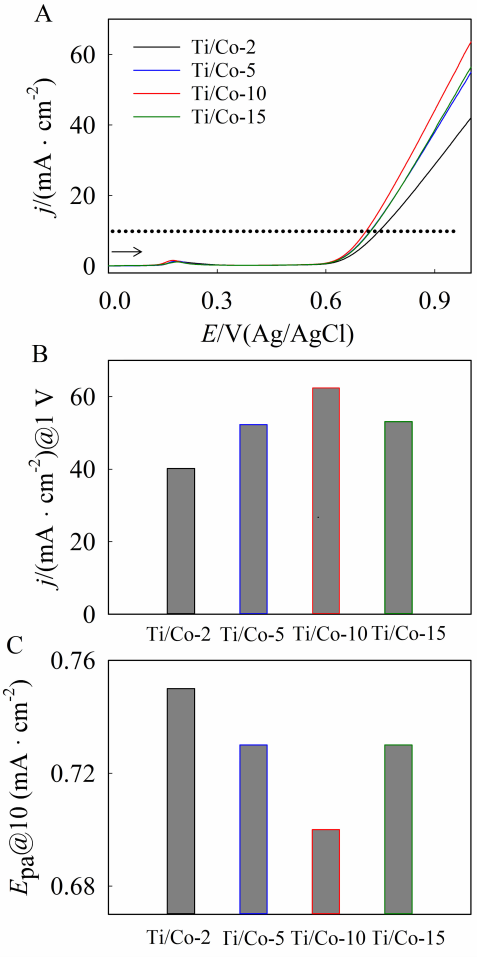

Fig. 4　A. LSV curves of the Ti/Co-2, Ti/Co-5, Ti/Co-10 and Ti/Co-15 electrodes recorded in 0.1 mol·L^{-1} KOH at a scan rate of 20 mV·s^{-1}; B-C. The current density plots at 1.0 V and E_{pa} at 10 mA·cm^{-2} against the Ti/Co electrodes.

Tab. 1 Comparison of OER parameters of the Ti/Co electrodes fabricated at different electrodeposition time

Electrode	Onset OER/V	E_{pa} OER/V@10 (mA·cm^{-2})	Tafel slope/ (mV·dec^{-1})	Overpotential/V
Ti/Co-2	0.58	0.75	85.70	0.46
Ti/Co-5	0.57	0.73	82.40	0.46
Ti/Co-10	0.56	0.70	81.10	0.43
Ti/Co-15	0.57	0.73	82.50	0.46

C_{dl} when CPE-P =1[31]. The CPE indicates the capacitive behavior of the interface at the Ti/Co electrode and the alkaline electrolyte. The resulting fitting curves are presented in Fig. 5 as solid lines, and the values of the R_s, R_p, CPE-T, and CPE-P elements with their associated errors (%) are listed in Table 2, demonstrating that the proposed equivalent electric circuit fits the EIS data very well. The R_s values for all of the electrodes used in this investigation were similar, in the range of 4.97 to 6.63 Ω·cm^2. The R_p values of the Ti electrodes modified with Co NPs with the electrodeposition time of 2, 5, 10, and 15 min were found to be 157.00, 125.60, 100.90, and 131.60 Ω·cm^2, respectively, which was consistent with the results presented in Fig. 4. The CPE-P values were also similar, in the range from 0.80 to 0.92 for all the electrodes. The CPE-T element values were found to be 8.18, 8.27, 8.68, and 8.34 mF·cm^{-2}

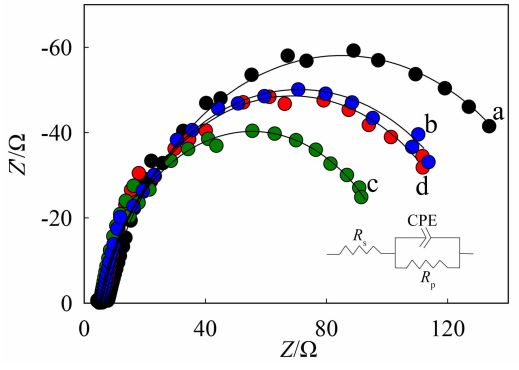

Fig. 5 Nyquist plots of the Ti/Co-2 (a), Ti/Co-5 (b), Ti/Co-10 (c) and Ti/Co-15 (d) electrodes recorded in 0.1 mol·L^{-1} KOH at an applied potential of 0.6 V. The amplitude of modulation potential was 5 mV. The frequency was changed from 100 kHz to 0.04 Hz. The inset is the corresponding equivalent electric circuit.

for the Ti/Co-2, Ti/Co-5, Ti/Co-10, and Ti/Co-15 electrodes, respectively. The lowest R_p and the largest CPE-T values further confirmed that the Ti/Co-10 electrode possessed the highest electrochemical activity toward OER in an alkaline electrolyte.

Tafel plots were obtained to further investigate the OER kinetics of the Ti/Co electrodes. Fig. 6 displays the Tafel plots of the Ti/Co-2 (black), Ti/Co-5 (red), Ti/Co-10 (green), and Ti/Co-15 (blue) electrodes recorded in 0.1 mol·L^{-1} KOH at a scan rate of 0.1 mV·s^{-1}. The resulting Tafel slopes were found to be 85.7, 82.4, 81.1, and 82.5 mV·dec^{-1} for the Ti/Co-2, Ti/Co-5, Ti/Co-10, and Ti/Co-15 electrodes, respectively, which were quite small, showing that all of the prepared Ti/Co electrodes possessed high catalytic activity for the OER. The Tafel slope was decreased from ~ 85.7 to 81.1 mV·dec^{-1} by lengthening the electrodeposition time, from 2 to 10 min. When the electrodeposition time was further increased, the Tafel slope was increased slightly to 82.5 mV·dec^{-1}, which further confirmed that 10 min was the optimum electrodeposition time. A small Tafel slope is desirable for practical water splitting applications as it may provide an increased OER rate with a decrease of the overpotential. It is noteworthy to note that the aforementioned voltammetric, impedance and Tafel plot results were consistent, indicating that the Co NPs possessed high catalytic activity for OER and that the increase of the current density was likely due to the increase of the electrochemically active surface area (EASA) when the deposition time was increased from 2 min to 10 min. Further prolonging the deposition time from 10 to 15 min, the EASA might be de creased due to the formation of larger particles.

Tab. 2 EIS fitting results from the Nyquist plots of Fig. 5 using a proposed equivalent electric circuit

Electrode	R_s/(Ω·cm^{-2})		R_p/(Ω·cm^{-2})		CPE-T/(mF·cm^{-2})		CPE-P	
	Value	Error/%	Value	Error/%	Value	Error/%	Value	Error/%
Ti/Co-2	6.63	0.90	157.00	1.20	8.18	2.30	0.80	0.27
Ti/Co-5	5.79	1.23	125.60	0.87	8.27	1.28	0.92	0.45
Ti/Co-10	4.97	2.03	100.90	1.03	8.68	2.08	0.89	0.78
Ti/Co-15	5.23	0.87	131.60	2.04	8.36	1.89	0.91	0.53

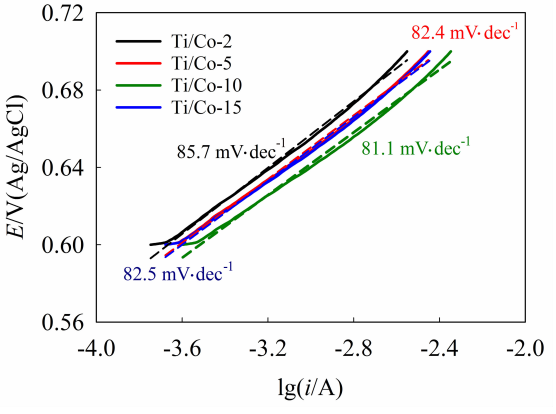

Fig. 6 Tafel plots of the Ti/Co-2, Ti/Co-5, Ti/Co-10 and Ti/Co-15 electrodes recorded in 0.1 mol·L^{-1} KOH at a scan rate of 0.1 mV·s^{-1}

The overpotentials of all the Ti/Co electrodes were calculated and are listed in Table 3. The Ti/Co-10 electrode exhibited the lowest overpotential (0.43 V), which was the lowest in comparison to most of the recent electrocatalysts summarized in Table 3. Mass activity is an important parameter of catalysts for practical applications. The mass activity (A·g^{-1}) of the optimized Ti/Co-10 electrode can becalculated using Equation (1):

$$\text{Mass activity} = j/m \quad (1)$$

where 'j' is the obtained current density (10 mA·cm^{-2}) at an overpotential (η) 0.43 V, and 'm' is the mass of the Co NPs deposited on the Ti substrate at the electrocatalyst, which was 0.0946 mg·cm^{-2}. The mass activity of the Ti/Co-10 electrode was calculated to be 105.7 A·g^{-1} at η = 0.43 V.

Based on the literature[20, 32], the reactions associated with OER mechanism that occurred at the catalyst (M) might be proposed as follows:

$$M + OH^- \rightarrow M\text{-}OH + e$$

$$M\text{-}OH + OH^- \rightarrow M\text{-}O + e + H_2O$$

$$M\text{-}O + OH^- \rightarrow M\text{-}OOH + e$$

$$M\text{-}OOH + OH^- \rightarrow M\text{-}O_2 + e + H_2O$$

$$M\text{-}O_2 \rightarrow M + O_2$$

The OER begins with the adsorption and discharge of hydroxyl anions (OH^-) at the catalyst. The formation of adsorbed hydroxide, atomic oxygen, and superoxy (OOH) species may take place at the electrode/electrolyte interface and four-electron transfer is involved in the overall oxygen evolution reaction. The forma-

Tab. 3 Comparison of the OER activity with different electrocatalysts reported in the literature

Electrode	Overpotential/V	Tafel slope/(mV·dec^{-1})	Electrolyte	Refs
FTO/NiP	0.50	60	1 mol·L^{-1} KOH	[33]
GC/CoP	0.49	77	1 mol·L^{-1} KOH	[34]
NF/NiSe@NiOOH	0.46	-	1 mol·L^{-1} KOH	[35]
GC/Ni_6(PET)	0.47	69	1 mol·L^{-1} KOH	[36]
GC/$Au_{71}Co_{29}$/C	0.52	66	0.1 mol·L^{-1} KOH	[37]
GC/Pt-C	0.56	127	0.1 mol·L^{-1} KOH	[15]
Ti/Co-10	0.43	81	0.1 mol·L^{-1} KOH	This work

FTO: fluorine doped tin oxide; GC: glassy carbon; NF: nickel foam

tion of M-OOH is considered as the rate-determining step; and a good electrocatalyst is expected to promote the formation of M-OOH as well as to facilitate the followed deprotonation step. The catalytic OER ability was further assessed by the turnover frequency (TOF) of the catalyst at this overpotential, which was estimated using Equation (2) by assuming that all the Co atoms were involved in the catalytic process[15]:

$$TOF = (j \times S)/(4Fn) \quad (2)$$

Herein, 'j' is the measured current density at η = 0.43 V; 'S' is the surface area of the Ti substrate; 4 is the four-electron transfer required for the formation of O_2; 'F' is Faraday's constant; and 'n' relates to the number of moles of Co atoms deposited on the Ti electrode surface. The TOF of the Ti/Co-10 electrode was calculated to be 1.63 × 10^{-3} s^{-1}, which was close to the value of the 20wt% Pt/C.

To develop cost-effective catalysts for OER, stability and reproducibility are also critical factors aside from their catalytic activity. The stability of the Ti/Co-10 electrode toward the OER was further investigated in 0.1 mol·L^{-1} KOH thought the application of a constant current density of 10 mA·cm^{-2} for 60,000 s using chronopotentiometry (Fig. 7). As shown in Fig. 7, the as-prepared Ti/Co-10 electrode demonstrated high stability, suggesting that the present inexpensive electrode was very appropriate for OER in an alkaline solution. Fig. 8A and Fig. 8B present the SEM images of the Ti/Co-10 electrode prior to and following the stability test, respectively. The rough surface of the Ti substrate seen in the SEM images was due to the HCl etching process as described in the experimental section. As displayed in Fig. 8, no obvious change in surface morphology of Co NPs was observed after the stability test carried at a constant current density of 10 mA·cm^{-2} for 60,000 s, further confirming that the developed Ti/Co-10 electrode possessed a high stability for the OER. Finally, the reproducibility of the Ti/Co electrodes was examined by employing three different electrodes that were fabricated and tested under identical conditions. The relative standard deviation (RSD) was measured at a current density of 10.0 mA·cm^{-2} to be 1.7%, which vali

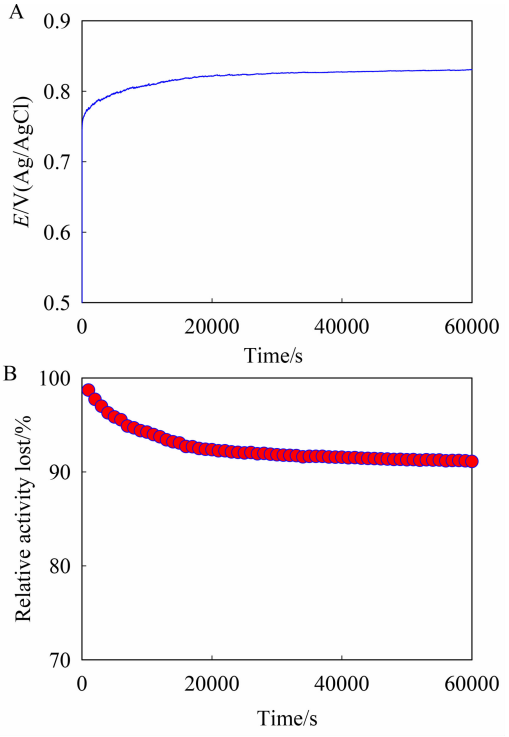

Fig. 7 Chronopotentiometric response (A) and relative catalytic activity (B) of the Ti/Co-10 electrode toward OER with an applied current density of 10.0 mA·cm^{-2} in 0.1 mol·L^{-1} KOH

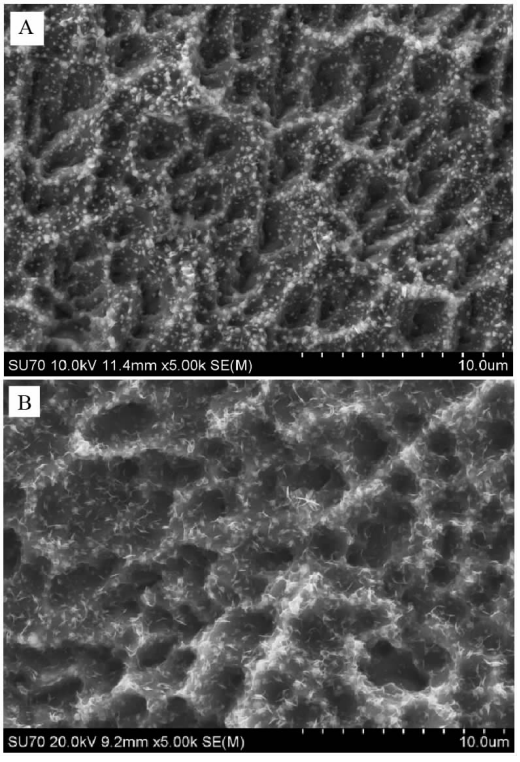

Fig. 8 SEM images of the Ti/Co-10 electrode prior to (A) and following (B) the stability test described in Fig. 7

dates an acceptable reproducibility of the optimized Ti/Co electrode for OER in 0.1 mol·L^{-1} KOH.

3 Conclusions

In summary, we have demonstrated a facile one-step electrochemical deposition approach for the fabrication of inexpensive, earth abundant, and non-noble metal electrocatalysts, including Fe, Ni, Co, CoNi, and CoFe NPs, which were directly formed on the Ti substrates for electrocatalytic water oxidation in an alkaline solution. Among the five synthesized nanoparticles, the Co NPs exhibited the highest electrocatalytic activity toward OER in 0.1 mol·L^{-1} KOH. The electrodeposition time was also optimized for the fabrication of the Ti/Co electrodes. A high mass activity, small Tafel slope and R_p value, low onset potential and overpotential, and large CPE-T were achieved on the optimized Ti/Co-10 electrode. The excellent OER activity of the Ti/Co electrode may have been attributed to the formation of highly densed and interconnected Co NPs on the Ti surface, which provided extensive catalytic active sites and enabled rapid electron transfer for the water oxidation reaction. Chronopotentiometric tests of the Ti/Co electrode revealed that the Co NPs, which were directly deposited on the Ti substrate, possessed high durability toward OER. The environmentally compatible fabrication process and easy scale-up to the massive production of the Ti/Co electrode with high catalytic activity, high stability, and low cost, make the strategy proposed in the present study promising for the development of high-performance OER electrocatalysts inpractical industrial energy conversion.

Acknowledgements

This research was supported by the Discovery Grant from the Natural Sciences and Engineering Research Council of Canada (NSERC RGPIN-2015-06248). A. Chen acknowledges NSERC and the Canada Foundation for Innovation (CFI) for the Canada Research Chair Award in Materials and Environmental Chemistry.

References:

[1] Govindhan M, Chen A. Novel cobalt quantum dot/graphene nanocomposites as highly efficient electrocatalysts for water splitting[J]. Nanoscale, 2016, 8(3): 1485-1492.

[2] Katsounaros I, Cherevko S, Zeradjanin A R, et al. Oxygen electrochemistry as a cornerstone for sustainable energy conversion[J]. Angewante Chemie International Edition, 2014, 53(1): 102 - 121.

[3] Liu Y L, Chen C C, Zhang N, et al. Research and application of key materials for sodium-ion batteries[J]. Journal of Electrochemistry, 2016, 22(5): 437-452.

[4] Perez-Alonso F J, Adan C, Rojas S, et al. Ni/Fe electrodes prepared by electrodeposition method over different substrates for oxygen evolution reaction in alkaline medium [J]. International Journal of Hydrogen Energy 2014, 39: 5204-5212.

[5] LeRoy R L, Stuart A K, Srinivasan S, et al. Ed. Industrial water electrolysis[M]. The Electrochemical Society,1978: 117.

[6] Walter M G, Warren E L, McKone J R, et al. Solar water splitting cells[J]. Chemical Review, 2010, 110(11): 6446-6473.

[7] Pu Z, Luo Y, Asiri A M, et al. Efficient electrochemical water splitting catalyzed by electrodeposited nickel diselenide nanoparticles based film[J]. ACS Applied Materials Interfaces, 2016, 8(7): 4718-4723.

[8] Bian W, Yang Z, Strasser P, et al. A $CoFe_2O_4$/graphene nanohybrid as an efficient bi-functional electrocatalyst for oxygen reduction and oxygen evolution[J]. Journal of Power Sources, 2014, 250: 196-203.

[9] Chen X. Mini-review: possible applications of scanning electrochemical microscopy (SECM) in characterizations of oxygen reduction reaction and oxygen evolution reaction[J]. Journal of Electrochemistry, 2016, 22(2): 113-122.

[10] Chao S, Geng M. 3,5-Diamino-1,2,4-triazole as a nitrogen precursor to synthesize highly efficient Co-N/C non-precious metal bifunctional catalyst for oxygen reduction reaction and oxygen evolution reaction[J]. International Journal of Hydrogen Energy, 2016, 41(30): 12995-13004.

[11] Jiao F, Frei H. Nanostructured cobalt oxide clusters in mesoporous silica as efficient oxygen-evolving catalysts [J]. Angewante Chemie International Edition, 2009, 48(10): 1841-1844.

[12] Kanan M W, Nocera D G. *In situ* formation of an oxygen-evolving catalyst in neutral water containing phosphate and Co^{2+}[J]. Science, 2008, 321(5892): 1072-1075.

[13] Chen S, Thind S S, Chen A. Nanostructured materials for water splitting - state of the art and future needs: A mini-review[J]. Electrochemistry Communications, 2016, 63: 10-17.

[14] McCrory C C L, Jung S, Ferrer I M, et al. Benchmarking

hydrogen evolving reaction and oxygen evolving reaction electrocatalysts for solar water splitting devices[J]. Journal of American Chemical Society 2015, 137(13): 4347-4357.

[15] Gao M R, Cao X, Gao Q, et al. Nitrogen-doped graphene supported $CoSe_2$ nanobelt composite catalyst for efficient water oxidation[J]. ACS Nano, 2014, 8(4): 3970-3978.

[16] Yang T, Dong W, Yang H, et al. Preparation and proper ties of binary oxides $Co_xCr_{1-x}O_{3/2}$ electrocatalysts for oxygen evolution reaction[J]. Journal of Electrochemistry, 2015, 21(2): 187-192.

[17] Wang L, Lin C, Huang D, et al. A comparative study of composition and morphology effect of $Ni_xCo_{1-x}(OH)_2$ on oxygen evolution/reduction reaction[J]. ACS Applied Materials Interfaces 2014, 6(13): 10172-10180.

[18] Chemelewski W D, Lee H C, Lin J F, et al. Amorphous FeOOH oxygen evolution reaction catalyst for photoelectrochemical water splitting[J]. Journal of American Chemical Society, 2014, 136(7): 2843-2850.

[19] Huang J, Xu Z, Li H, et al. Electrochemical studies of iron-doped nickel oxide electrode for oxygen evolution reaction[J]. Journal of Electrochemistry, 2006, 12(2): 154-158.

[20] Yeo B S, Bell A T. Enhanced activity of gold-supported cobalt oxide for the electrochemical evolution of oxygen [J]. Journal of American Chemical Society, 2011, 133 (14): 5587-5593.

[21] Ling C, Zhou L Q, Jia H. First-principles study of crys talline $CoWO_4$ as oxygen evolution reaction catalyst[J]. RSC Advances, 2014, 4(47): 24692-24697.

[22] Wang J, Qiu T, Chen X, et al. Hierarchical hollow urchin-like $NiCO_2O_4$ nanomaterial as electrocatalyst for oxygen evolution reaction in alkaline medium[J]. Journal of Power Sources 2014, 268: 341-348.

[23] Doyle R L, Lyons M E G. Redox and oxygen evolution electrocatalytic properties of Nafion and single-walled carbon nanotube/hydrous iron oxide composite films[J]. Electrocatalysis, 2014, 5(4): 114-124.

[24] Mellsop S R, Gardiner A, Marshall A T, et al. Electrocatalytic oxygen evolution on electrochemically deposited cobalt oxide films: Comparison with thermally deposited films and effect of thermal treatment[J]. Electrocatalysis, 2015, 5(4): 445-455.

[25] Suryanto B H R, Lu X, Zhao C. Layer-by-layer assembly of transparent amorphous CO_3O_4 nanoparticles/graphene composite electrodes for sustained oxygen evolution reaction[J]. Journal of Material Chemistry A, 2013, 1(41): 12726-12731.

[26] Zhou X, Xia Z, Zhang Z, et al. One-step synthesis of multi-walled carbon nanotubes/ultra-thin $Ni(OH)_2$ nanoplate composite as efficient catalysts for water oxidation [J]. Journal of Material Chemistry A, 2014, 2(30): 11799-11806.

[27] Chen A, Chatterjee S. Nanomaterials based electrochemical sensors for biomedical applications[J]. Chemical Society Reviews 2013, 42(12): 5425-5438.

[28] Adhikari B R, Govindhan M, Chen A. Sensitive detection of acetaminophen with graphene-based electrochemical sensor[J]. Electrochimica Acta, 2015, 162:198-204.

[29] Govindhan M, Chen A. Simultaneous synthesis of gold nanoparticle/graphene nanocomposite for enhanced oxygen reduction reaction[J]. Journal of Power Sources 2015, 274: 928-936.

[30] Yao Y, Xu C, Qin J, et al. Synthesis of magnetic cobalt nanoparticles anchored on graphene nanosheets and catalytic decomposition of orange II[J]. Industrial Engineering Chemistry Research, 2013, 52(49): 17341-17350.

[31] Chen A, Russa D J L, Miller B. Effect of the iridium oxide thin film on the electrochemical activity of platinum nanoparticles[J]. Langmuir, 2004, 20(22): 9695-9702.

[32] Lyons M E G, Brandon M P A. Comparative study of the oxygen evolution reaction on oxidised nickel, cobalt and iron electrodes in base[J]. Journal of Electroanalytical Chemistry, 2010, 641(1/2): 119-130.

[33] Han A, Chen H L, Sun Z J, et al. High catalytic activity for water oxidation based on nanostructured nickel phosphide precursors[J]. Chemical Communications, 2015, 51 (58): 11626-11629.

[34] Liu M, Li J. Cobalt phosphide hollow polyhedron as efficient bifunctional electrocatalysts for the evolution reac tion of hydrogen and oxygen[J]. ACS Applied Materials Interfaces, 2016, 8(3): 2158-2165.

[35] Li X, Han G Q, Liu YR, et al. NiSe@NiOOH core-shell hyacinth-like nanostructures on nickel foam synthesized by *in situ* electrochemical oxidation as an efficient electrocatalyst for the oxygen evolution reaction[J]. ACS Applied Materials Interfaces,2016, 8(31): 20057-20066.

[36] Kauffman D R, Alfonso D, TafenD N, et al. Electrocatalytic oxygen evolution with an atomically precise nickel catalyst[J]. ACS Catalysis, 2016, 6(2): 1225-1234.

[37] Lu A, Peng D L, Chang F, et al. Composition- and structure-tunable gold-cobalt nanoparticles and electrocatalytic synergy for oxygen evolution reaction[J]. ACS Applied Materials Interfaces, 2016, 8(31): 20082-20091.

用于电化学水氧化的铁、镍、钴金属及其二元金属纳米颗粒比较研究

Maduraiveeran Govindhan, Brennan Mao, 陈爱成*

(加拿大湖首大学化学系, 桑德贝, 安大略 P7B 5E1)

摘要： 从环境兼容角度来设计应用于氧析出反应的电催化剂是否有效、耐用和廉价对能源转化过程至关重要. 本文报告了一种快速制备低成本、原料丰富的金属催化剂制备方法. 通过一步电化学沉积法在钛金属基材上制备了铁、镍、钴金属及其钴镍、钴铁二元金属纳米颗粒. 采用场发射电子显微镜(FE-SEM)、能量散射 X- 射线能谱(EDX)、X- 射线衍射光谱(XRD)、X- 射线光电子能谱(XPS)和电化学技术对制备的不同纳米颗粒进行了表征. 电化学结果显示, 在合成的五种钛基金属纳米催化剂中, 钛基上沉积钴金属纳米颗粒(Ti/Co)电极在 0.1 mol·L^{-1} 氢氧化钾溶液中氧析出反应的电催化活性最好, 0.70 V (相对于银/氯化银电极) 的电流密度为 10.0 mA·cm^{-2}. 经优化后 Ti/Co 电极的过电位(η)很小, 当电流密度为 10.0 mA·cm^{-2} 时 η 为 0.43 V, 质量活性高达 105.7 A·g^{-1}, 逆转频率(TOF)值为 1.63×10^{-3} s^{-1}, 这些与当前最好的碳载铂(Pt/C)和氧化钌(RuO_2)电催化剂的性能相当. 此外, 通过计时电位技术对优化后 Ti/Co 电极的耐久性进行了测试, 发现该电极在碱性溶液中氧析出反应的稳定性良好. 本工作制备的钛金属基材上电化学沉积金属钴纳米颗粒具有高催化活性、高稳定性、原料来源丰富、廉价且易于大规模生产, 在工业化水分解领域具有潜在的应用前景.

关键词： 钴纳米颗粒; 电化学沉积; 电催化剂; 氧气析出反应; 能量转换